ACS Catalysis

Research Article

pubs.acs.org/acscatalysis

# Yin and Yang Dual Characters of $CuO_x$ Clusters for C−C Bond Oxidation Driven by Visible Light

Tingting Hou,[†,‡] Nengchao Luo,[†,‡] Hongji Li,[†,‡] Marc Heggen,[§] Jianmin Lu,[†] Yehong Wang,[†] and Feng Wang*[,†]

[†]State Key Laboratory of Catalysis, Dalian National Laboratory for Clean Energy, Dalian Institute of Chemical Physics, Chinese Academy of Sciences, Dalian 116023, People's Republic of China

[‡]University of Chinese Academy of Sciences, Beijing 100049, People's Republic of China

[§]Ernst Ruska Centre for Microscopy and Spectroscopy with Electrons and Peter Grünberg Institute, Forschungszentrum Juelich GmbH, Juelich 52425, Germany

Supporting Information

**ABSTRACT:** Selective cleavage of C−C bonds is pursued as a useful chemical transformation method in biomass utilization. Herein, we report a hybrid $CuO_x$/ceria/anatase nanotube catalyst in the selective oxidation of C−C bonds under visible light irradiation. Using the lignin $\beta$-1 model as a substrate offers 96% yields of benzaldehydes. Characterization results by high angle annular dark field scanning transmission electron microscopy (HAADF-STEM) and energy-dispersive X-ray spectroscopy element (EDX) mapping reveal that $CuO_x$ clusters are highly dispersed on the exposed anatase surface as well as on the nanosized ceria domains. In-depth investigations by Raman and ultraviolet visible diffuse reflectance spectra (UV−vis DRS), together with density functional theory (DFT) calculations, further verify that the $CuO_x$ clusters present on the ceria domains increase the concentration of surface defects ($Ce^{3+}$ ions and oxygen vacancies) and accordingly improve the photocatalytic activity (Yang character); the $CuO_x$ clusters decorating on anatase suppress the side reaction (oxy-dehydrogenation without C−C bond cleavage) because of an upward shift in the valence band (VB) edge of anatase (Yin character). Mechanism investigation indicates hydrogen abstraction from $\beta$-carbon by photogenerated holes is a vital step in the conversion.

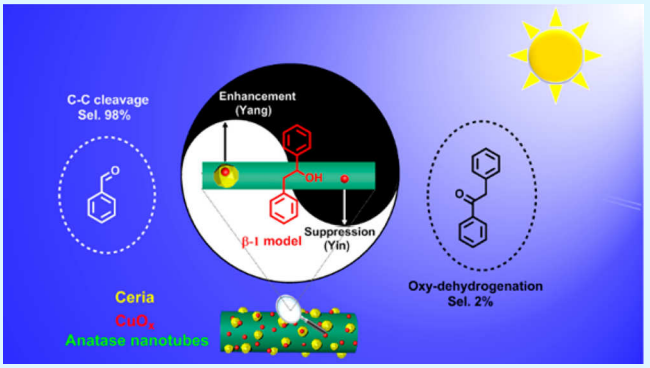


**KEYWORDS:** *heterogeneous catalysis, visible light, ceria, copper, titania, C−C bond, benzaldehyde*

## INTRODUCTION

The selective oxidation of C−C bonds is a significant process to produce oxygenates.[1] As an alternative and sustainable feedstock, lignin accounts for around 30% of the weight of lignocellulosic biomass.[2] The presence of C−C bonds is one of the reasons for lignin's recalcitrance to be converted into monomers. As a typical C−C bond, the $\beta$-1 linkage connects two phenyl groups by replacement of the O-bound phenoxy unit with a C-bound aryl group (Scheme 1). Baker, Hanson, et al. have reported the cleavage of $\beta$-1 bonds over a copper(I) trifluoromethanesulfonate catalyst assisted by 10 mol % of 2,2,6,6-tetramethyl-1-piperidinyloxy (TEMPO) and 10 equiv of 2,6-lutidine.[3] Shi's group has developed a protocol to fragment lignin $\beta$-1 models using sodium persulfate as an oxidant at 100 °C.[4] Very recently, our group has reported a $Cu(OAc)_2/BF_3{\cdot}OEt_2$ catalytic system for C−C bond cleavage in $\beta$-1 ketones.[5] However, a facile and efficient catalytic system that can achieve the lignin $\beta$-1 C−C bond cleavage is desired but far less developed.

Photocatalytic processes hold great promise in reducing the energy consumption in organic reactions[6] and have attracted broad interest.[7] These processes will be of significance to realize the photolysis of lignin into monomers under mild conditions.[8] When a C−C bond is a targeted linkage to be cleaved, the activation of the $C_\beta$−H bond is a requisite (Scheme 1).[9] However, once the C−OH bond is converted to a ketone via oxy-dehydrogenation, the $C_\alpha$−$C_\beta$ bond dissociation energy (BDE) increases from 294.7 to 354.2 kJ/mol, and consequently the ketone formed is more difficult to convert. This is different from the cleavage of the $\beta$-O-4 bond, which is easier to cleave once the C−OH bond is preoxidized to a ketone.[8a,10] Thus, a highly selective catalyst to oxidize $\beta$-1 C−C bonds should selectively activate $C_\beta$−H bonds but suppress the formation of

Received: February 24, 2017
Revised: April 19, 2017
Published: April 24, 2017

  

DOI: 10.1021/acscatal.7b00629
ACS Catal. 2017, 7, 3850−3859

**Scheme 1. Oxy-Dehydrogenation Reaction Competes with C−C Cleavage Reaction in the Oxidation of $\beta$-1 Model**

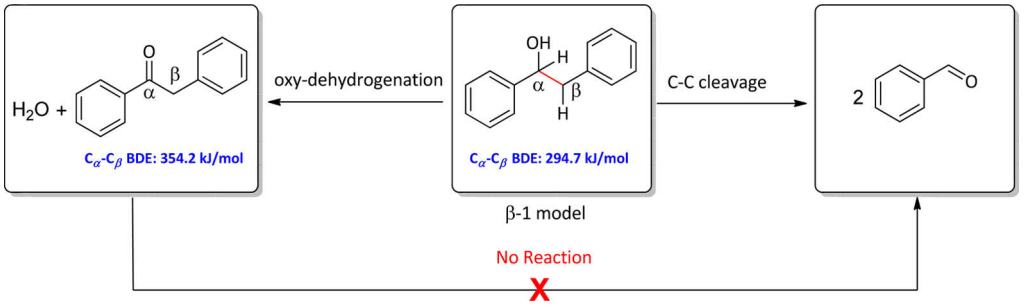


ketone. This has rarely been achieved in heterogeneous photocatalysis.[11]

We herein report the bifunctionality of $CuO_x$ clusters in the photolysis of C−C bonds, especially in the lignin $\beta$-1 model. Catalytic results show that decoration of $CuO_x$ clusters on ceria/anatase significantly promotes C−C bond cleavage with 98% selectivity of benzaldehyde under visible light. The reaction mechanism involves hydrogen abstraction from a benzylic carbon ($\beta$-C) by the photogenerated holes, which is supported by control experiments and kinetic isotope effect (KIE) investigations. Detailed studies, including X-ray diffraction (XRD), HAADF-STEM, EDX mapping, physical absorption, and Raman and UV−vis DRS as well as DFT calculations, reveal that the highly dispersed $CuO_x$ clusters have dual characters on both ceria domains and exposed anatase nanotubes: i.e., promoting the C−C bond cleavage (Yang character) and inhibiting unwanted oxy-dehydrogenation reactions (Yin character).[12] This study attains selective C−C bond oxidation to benzaldehydes, particularly in the presence of competitive ketone formation reaction, using photoenergy by controlling the decoration location of $CuO_x$ clusters. Although copper catalysts have been known to activate C−C bonds,[9b] such dual characters of $CuO_x$ clusters in heterogeneous catalysis are very rare.

## EXPERIMENTAL SECTION

**Chemicals and Materials.** All chemicals were of analytical grade, purchased from Aladdin Chemicals Co. Ltd. (Shanghai, People's Republic of China) and used without further purification.

**Catalyst Preparation.** $TiO_2$ nanotubes were synthesized by a hydrothermal approach, which has been described in detail elsewhere.[13] Briefly, 5 g of $TiO_2$ (anatase) powder was dispersed in 70 mL of 10 M NaOH with stirring. The mixture was then transferred into a 150 mL Teflon-lined autoclave. The autoclave was then sealed and placed in a preheated oven at 140 °C for 20 h. The precipitated powder was filtered and washed several times with 0.1 M $HNO_3$ and deionized water until the filtrate solution became neutral. Then it was air-dried at 105 °C overnight. The resulting product was denoted as A-NTs. The rutile nanotubes (R-NTs) were prepared by the same procedure.

The ceria sample was prepared by a conventional precipitation method reported by our group.[14] Briefly, 5.0 g of $Ce(NO_3)_3{\cdot}6H_2O$ was dissolved in 100 mL of Millipore-purified water (18 mΩ cm), and the solution was adjusted to pH 10.0 by the addition of $NH_3{\cdot}H_2O$ with magnetic stirring at room temperature. The resulting gel mixture was washed with pure water, dried in an oven at 120 °C overnight, and calcined at 400 °C in air for 6 h.

For ceria/A-NT, $CuO_x$/A-NT, and $CuO_x$/ceria/A-NT nanocomposites, a wet-chemical deposition precipitation (DP) method was employed. The preparation procedure was as follows: 0.87 g of $Ce(NO_3)_3{\cdot}6H_2O$ was dissolved in 100 mL of Millipore-purified water and mixed with 1.6 g of the as-prepared anatase nanotubes. Sufficient $NH_3{\cdot}H_2O$ (25−28 wt %) was then added with vigorous stirring to adjust the pH to 10. After that, this mixture was stirred again for 5 h and then aged for 4 h without stirring at room temperature. The resulting product was filtered, dried at 105 °C overnight, and calcined at 400 °C for 2 h to generate ceria/A-NTs. Other $TiO_2$-supported catalysts, such as $CuO_x$/A-NTs, $CuO_x$/ceria/A-NTs, and ceria/R-NTs, were prepared by the same wet-chemical DP method. Note that, for all of the catalysts, the Ce/Ti, Cu/Ce and Cu/Ti molar ratios were 1/10, 1/4, and 1/40, respectively.

**Catalyst Characterizations.** Powder X-ray diffraction patterns were conducted on a PANalytical X-Pert PRO diffractometer, using Cu K$\alpha$ radiation at 40 kV and 20 mA. Continuous scans were collected in the $2\theta$ range of 10−80°.

Scanning transmission electron microscopy (STEM) was performed using a FEI Titan 80-200 (ChemiSTEM) electron microscope operated at 200 kV, equipped with a spherical-aberration (Cs) probe corrector (CEOS GmbH) and a high-angle annular dark field (HAADF) detector. A probe semiangle of 25 mrad and an inner collection semiangle of the detector of 88 mrad were used. Compositional maps were obtained with energy-dispersive X-ray spectroscopy (EDX) using four large-solid-angle symmetrical Si drift detectors. For EDX analysis, Cu K, Ti K, and Ce L peaks were used. High-resolution transmission electron microscopy (HRTEM) investigations were performed using an FEI-Titan 80-300 electron microscope equipped with a Cs corrector for the objective lens. The microscope was operated at a voltage of 300 kV using the negative-Cs imaging technique (NCSI, with Cs set at around ~13 $\mu$m and defocus around +6 nm).

The Brunauer−Emmett−Teller (BET) surface areas, total pore volumes, and average pore sizes of the samples were measured by $N_2$ adsorption and desorption on a Quadrasorb SI instrument (Quantachrome, USA) at liquid nitrogen temperature (77.3 K). Before measurement, the sample was degassed under vacuum conditions at 300 °C for 5 h. The BET specific surface area was calculated from the adsorption data in the relative pressure range between 0.05 and 0.30.

Raman spectra were recorded on a confocal microscopic Raman spectrometer (Bruker Optics Senterra) using a laser with a wavelength of 532 nm.

UV−vis diffuse reflectance spectra were recorded on a JASCO V-550 UV−vis spectrophotometer.



DOI: 10.1021/acscatal.7b00629
ACS Catal. 2017, 7, 3850−3859

**Photocatalytic Activity Tests.** Photocatalytic aerobic oxidation reactions were carried out in a homemade LED photoreactor. Typically, 0.05 mmol of 1,2-diphenylethanol (substrate **1**) and 10 mg of photocatalyst were added to 1 mL of solvent in a 4 mL quartz tube. The system was replaced with $O_2$ for 1 min before it was sealed with a ground glass stopper and Parafilm. The quartz tube was then irradiated with 455 nm LED light. The conversion of 1,2-diphenylethanol and yield of benzaldehyde (**1a**) were determined by gas chromatography (GC) with *n*-dodecane as the internal standard. The selectivities of products were determined by GC-MS with the corresponding area percentage. *Caution! Specific protection by wearing eye goggles to shield 455 nm light is mandatory to avoid injuring eyes.*

**Computational Method of PEDOS.** All of the first-principles electronic structure calculations were carried out using the Vienna ab initio simulation package (VASP),[15] one density functional theory implementation. The exchange correlation potential was described by the Perdew–Burke–Ernzerhof (PBE)[16] formulation of the generalized gradient approximation (GGA). The ion–electron interactions were represented by the projector augmented wave (PAW)[17] method, while the valence electrons ($2s^2 2p^4$ of O, $3s^2 3p^6 3d^2 4s^2$ of Ti, and $3d^{10} 4s$ of Cu) were expanded by a plane wave basis set with an energy cutoff of 400 eV. The *k*-point sampling was performed using the Monkhorst–Pack scheme.[18] The electronic self-consistent minimization was converged to $10^{-5}$ eV, and the geometry optimization was converged to $10^{-4}$ eV. The self-interaction error (SIE) was mitigated using the DFT+U method by Dudarev and his colleagues.[19] A typical *U* value of 4.5 eV was used for Ti.

The lattice constants of anatase $TiO_2$ were optimized to be $a$ = 3.855 Å and $c$ = 9.661 Å, in good agreement with the experimental constants, $a$ = 3.782 Å and $c$ = 9.502 Å.[20] We used them to build a $p(2 \times 4)$ $TiO_2(101)$ slab with 12 atomic layers and a vacuum of 15 Å. Atoms in the bottom 6 atomic layers were fixed to their bulk positions, while the rest were allowed to fully relax. A 4 × 3 × 1 *k*-point mesh was used.

**Computational Method of BDE.** The Vienna ab initio package (VASP)[21] was employed to perform spin-polarized DFT calculations within the generalized gradient approximation (GGA) using the PBE[22] functional formulation. The ionic cores were described by the projected augmented wave (PAW) pseudopotentials.[23] 1s of H, $2s^2 2p^2$ of C, and $2s^2 2p^4$ of O electrons were explicitly taken into account using a plane wave basis set with an energy cutoff of 400 eV. Partial occupancies of the Kohn–Sham orbitals were allowed using the Gaussian smearing method and a width of 0.05 eV. All of the molecules and radicals after bond cleavage were put separately and relaxed fully in a cubic box with a side length of 20 Å. Brillouin zone integration was performed using a 2 × 2 × 2 Monkhorst–Pack grid. The electronic energy was considered self-consistent when the energy change was $10^{-7}$ eV. A geometry optimization was considered convergent when the energy change was $10^{-6}$ eV.

## RESULTS AND DISCUSSION

**Photocatalytic Oxidation of Lignin *β*-1 Model.** We first explored the oxidation of 1,2-diphenylethanol under 455 nm visible light irradiation (Figure 1). The reaction did not proceed in the absence of catalyst. Pristine ceria exhibited moderate activity toward C–C bond cleavage of the *β*-1 lignin model under visible light and gave 35% conversion of substrate **1** with 98% selectivity of C–C bond cleavage. The photocatalytic

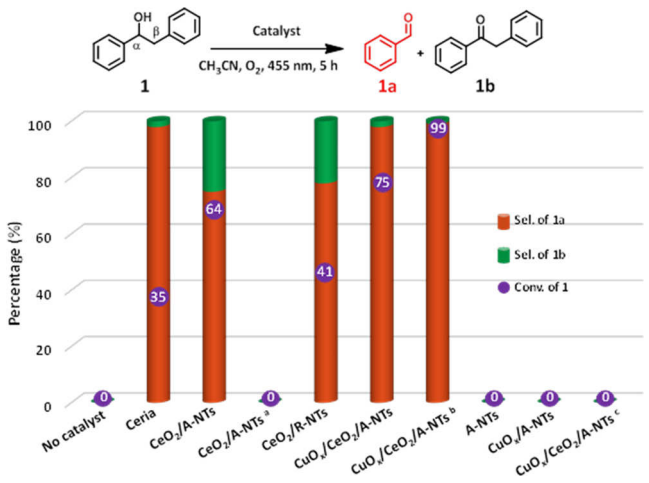


**Figure 1.** Photocatalytic activity of different photocatalysts for oxidation of substrate **1**. Reaction conditions: substrate **1** (0.05 mmol), catalyst (10 mg), $CH_3CN$ (1.0 mL), $O_2$ (1 atm), 9.6 W LED (centered at 455 nm), room temperature, 5 h. Legend: (a) with **1b** as substrate; (b) reaction time 10 h; (c) reaction conducted in the dark.

activity of ceria depends on the concentration of surface defect sites ($Ce^{3+}$ ions and O vacancies).[24] Tuning the surface defects could tailor the photoreactivity of ceria catalysts.[25] Aiming at achieving defected ceria, we dispersed ceria on anatase nanotubes (A-NTs) by a deposition–precipitation (DP) method with a Ce/Ti molar ratio of 1/10. The as-prepared ceria contained abundant $Ce^{3+}$ and oxygen vacancies at the exposed interface of ceria and anatase.[13b] Expectedly, the conversion of **1** over ceria/A-NTs reached 64%. Benzaldehyde was the major product. However, such a catalyst showed 25% selectivity of oxy-dehydrogenation to diphenylethanone (**1b**), indicating that the ceria/A-NT catalyst has oxy-dehydrogenation ability. Employing diphenylethanone (**1b**) as substrate gave no benzaldehyde, implying that the oxy-dehydrogenation reaction to ketone is parallel to the C–C cleavage reaction to benzaldehyde. Replacing the anatase nanotube support by rutile nanotubes decreased the conversion but did not increase selectivity.

In order to increase benzaldehyde selectivity, the parallel oxy-dehydrogenation reaction should be suppressed. Previous studies have shown that the modification with copper oxides could alter the photocatalytic activity of $TiO_2$.[26] On the other hand, the copper-based catalysts are favorable for thermal oxidative cleavage of C–C bonds, as reported by other groups and ours.[1d,9b,27] Therefore, we prepared a catalyst by mixing copper and cerium salt precursors and precipitating them on A-NTs by the DP method, denoted $CuO_x$/ceria/A-NTs (2 wt % CuO loading relative to ceria/A-NTs) for this reaction. The conversion of substrate **1** increased to 75%, surprisingly with 98% selectivity of benzaldehyde. Extension of the reaction time to 10 h realized complete conversion of substrate **1** with >99% selectivity of benzaldehyde. The oxy-dehydrogenation reaction was almost completely suppressed. Control reactions using A-NTs and $CuO_x$/A-NTs as catalysts under the same conditions gave no product,[28] indicating that ceria plays a key role in this photocatalytic system. Moreover, it is a photocatalytic reaction and did not occur in the dark.

We then investigated the photo-oxidation of a more complex *β*-1 model, 1-(3,4-dimethoxyphenyl)-2-(4-methoxyphenyl)-propane-1,3-diol (substrate **2**), with *γ*-hydroxyl and methoxyl


DOI: 10.1021/acscatal.7b00629
ACS Catal. 2017, 7, 3850–3859

**Scheme 2. Photocatalytic C−C Bond Cleavage of Nonphenolic Lignin Model Substrate 2 to Aromatic Aldehydes over $CuO_x$/Ceria/A-NTs[a]**

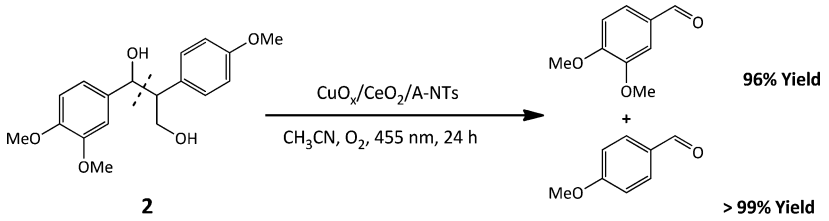


[a]Reaction conditions: substrate **2** (0.05 mmol), $CuO_x$/ceria/A-NTs (10 mg), $CH_3CN$ (1.0 mL), $O_2$ (1 atm), 9.6 W LED (centered at 455 nm), room temperature, 24 h. The yields of aldehydes were determined by GC with *n*-dodecane as the internal standard.

substituents (Scheme 2). The cleavage of C−C bonds offered a 96% yield of veratraldehyde and a >99% yield of anisic aldehyde even in the presence of γ-hydroxyl and methoxyl groups. The Cu/substrate ratio and temperature of reaction are lower and the yields of aromatic aldehydes are higher in comparison to those of a homogeneous copper catalyst.[3]

**XRD and TEM Characterization of the Photocatalysts.** Such unexpected results motivated us to investigate the structure of the catalysts. XRD diffraction patterns of the as-prepared ceria and A-NTs are dominated by the expected lines for *fcc* fluorite $CeO_2$ (JCPDS: 34-0394) and anatase (JCPDS: 21-1272), respectively (Figure 2). The characteristic peaks of

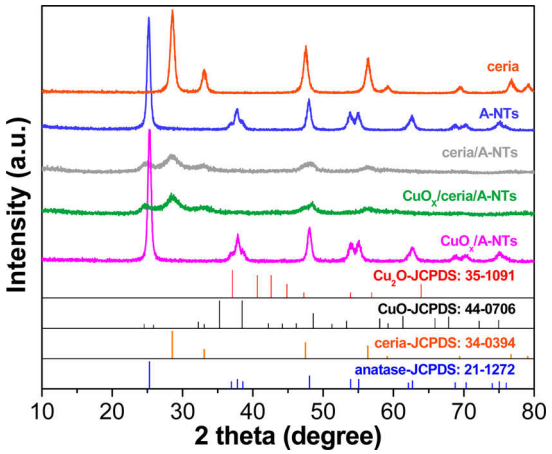


**Figure 2.** XRD patterns of ceria, A-NT, ceria/A-NT, $CuO_x$/ceria/A-NT, and $CuO_x$/A-NT photocatalysts, respectively.

crystalline ceria are not observed except for a weak and broad peak at 28.6° for ceria/A-NTs and $CuO_x$/ceria/A-NTs. It is well accepted that, if the size of crystalline particles is smaller than 4 nm, their diffraction peaks will be significantly broadened or even absent.[29] Therefore, the disappearance of ceria diffraction peaks is due to the high dispersion of ceria. After $CuO_x$ was decorated onto ceria/A-NTs or A-NTs (2 wt % respective to ceria/A-NTs), no extra diffraction lines attributed to $CuO_x$ were observed, indicating the high dispersion of $CuO_x$.

To investigate the microstructure of the photocatalysts, HRTEM, HAADF-STEM, EDX mapping, and fast Fourier transform (FFT) characterizations were then carried out (Figure 3 and Figure S1 in the Supporting Information). The as-prepared anatase sample has a nanotube structure with outer and inner diameters of about 10 and 6.5 nm, respectively (Figure S1a). The $CuO_x$/ceria/A-NTs consist of uniform and well-dispersed nanoparticles on the ridged surface of the anatase nanotubes. A comparison between the high-resolution STEM image (Figure 3d) and the EDX maps confirms that the bright dots are ceria nanoparticles. The size of the ceria ranged from 2 to 8 nm with an average diameter of 4.3 nm (Figure S1 and Figure 3). The FFT image in Figure 3b displays the interplanar *d* spacings for $CeO_2$ ($d_{111}$ = 0.31 nm), $TiO_2$ ($d_{101}$ = 0.35 nm), $Cu_2O$ ($d_{200}$ = 0.21 nm), and CuO ($d_{200}$ = 0.23 nm and $d_{110}$ = 0.28 nm) (Figure 3c), respectively. The STEM images and EDX mappings (Figure 3 and Figure S1d) confirm that Ce and Cu are highly dispersed on the $CuO_x$/ceria/A-NT substrate. Furthermore, the EDX maps (Figure 3e−i) show that the $CuO_x$ clusters are very finely dispersed and are associated with both ceria nanoparticles and the naked anatase nanotubes. The BET surface areas and pore volume measurements by nitrogen adsorption and desorption were also conducted (Table S1 in the Supporting Information). Both BET surface areas and pore volumes only have a slight decline for ceria/A-NTs and $CuO_x$/ceria/A-NTs in comparison with A-NTs, indicating that most of the ceria and $CuO_x$ are present on the exterior surface of the nanotubes.

**Investigation of the Reaction Mechanism.** Next, we turned our attention to elucidating the reaction mechanism. The effects of the reaction atmosphere and trapping agents were explored to discover the key active species that oriented the reaction path (Figure 4). When the reaction was conducted in air, the yield of benzaldehyde slightly decreased to 60% (Figure 4b). Moreover, the yield decreased to 9% under Ar (Figure 4c), indicating that oxygen is necessary. According to previous studies, molecular oxygen could be activated to a superoxide anion radical after acquiring an excited electron from the conduction band of a photocatalyst.[30] Adding 1 equiv of the superoxide anion radical scavenger *p*-benzoquinone (BQ)[30a] decreased the benzaldehyde yield to <1% (Figure 4d), inferring that this is a possible radical reaction.[30] Adding ammonium oxalate (AO)[30a] to capture photogenerated holes could reduce the benzaldehyde yield to 1% (Figure 4e). Adding $K_2S_2O_8$[30a] to capture photogenerated electrons also led to a low yield of benzaldehyde (6%) (Figure 4f). The above results suggest that photoexcited electrons, holes, and superoxide anion radicals are essential species for the reaction.

Diphenylethanone (**1b**) could be oxidized to an ester via C−C bond cleavage using $Cu(OAc)_2/BF_3{\cdot}OEt_2$ catalyst.[5] In this study, diphenylethanone could not be converted into benzaldehyde using the $CuO_x$/ceria/A-NTs catalyst (Scheme 3, eq 1). The results show that the oxy-dehydrogenation of **1** to **1b** competes with the C−C cleavage reaction. Furthermore, we investigated the H/D KIE of the reaction (Scheme 3). When **1-D** or **1′-D** was used as the substrate, secondary kinetic isotope effects with $k_H/k_D$ values of 1.44 and 1.23, respectively, were observed, indicating that the cleavage of the O−H or $C_\alpha$−H



DOI: 10.1021/acscatal.7b00629
ACS Catal. 2017, 7, 3850−3859

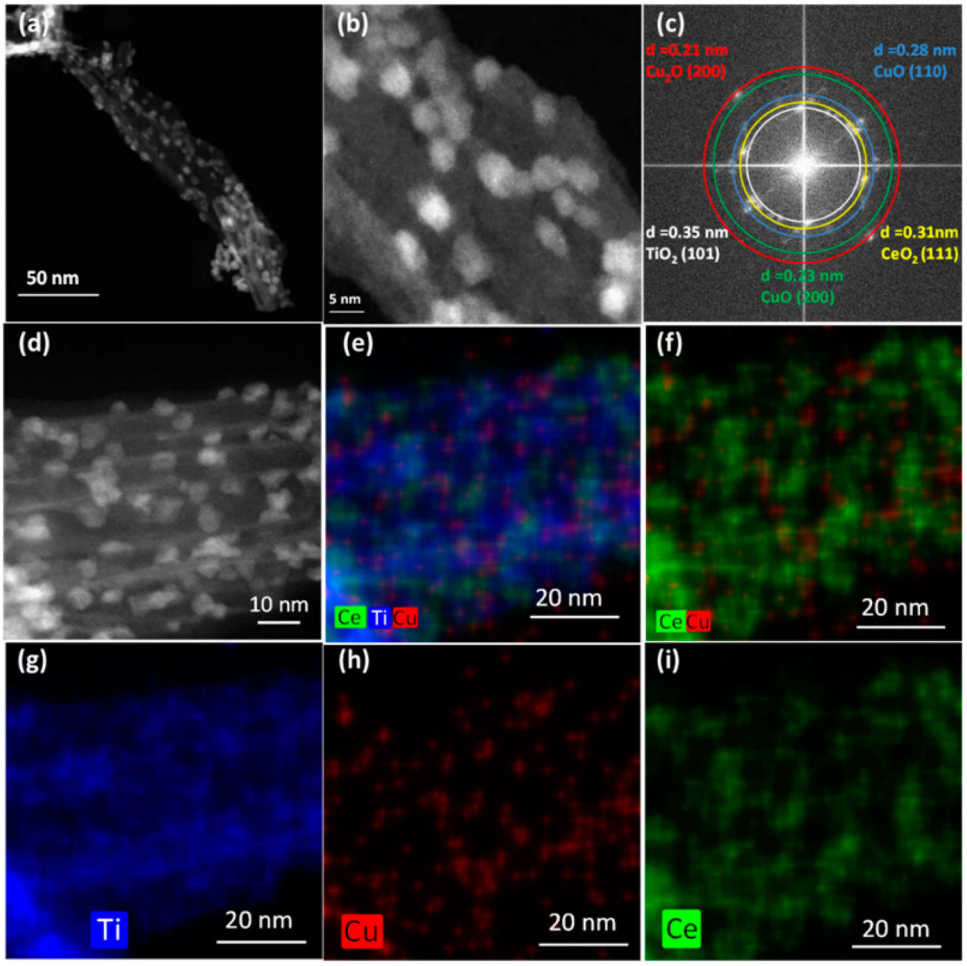


**Figure 3.** Low-resolution (a) and high-resolution (b) HAADF-STEM images. (c) Fast Fourier transform of image (b). (d) High-resolution HAADF-STEM image and corresponding (e–i) EDX maps of $CuO_x$/ceria/A-NTs.

bond is not a rate-determining step (Scheme 3, eqs 2 and 3). Notably, when using **1′-D** as substrate, nearly half of the benzaldehyde was deuterated (Scheme 3, eq 3). Further experiments showed that benzaldehyde could not undergo H/D exchange with 0.5 equiv of deuterated water under the reaction conditions (Scheme 3, eq 4). These results demonstrate that the $C_\alpha$–H bond connecting with the hydroxyl group was retained during the C–C bond cleavage. Additionally, a first-order KIE with a value of 6.53 was observed for **1″-D** (Scheme 3, eq 5), implying that the H abstraction from $\beta$-C is involved in the C–C bond cleavage of substrate **1**. Oxidation of **1** to **1a** and **1b** is distinguished on the basis of an initial hydrogen abstraction reaction at one of two positions ($\alpha$-C and $\beta$-C). A benzylic radical is generated at $\alpha$-C or $\beta$-C, which is resonance-stabilized by the aromatic ring.

On the basis of the above results, we propose a tentative reaction mechanism involving hydrogen abstraction at the $\alpha$ or $\beta$ position, as depicted in Scheme 4. A photogenerated electron is transferred to $O_2$, producing a superoxide anion radical. The hole abstracts a hydrogen from $\beta$-C to generate a $C_\beta$-centered radical. The superoxide anion radical then adds to a $C_\beta$-centered radical, forming an unstable peroxide intermediate. The latter will undergo $C_\alpha$–$C_\beta$ cleavage with the elimination of $H_2O$ to form benzaldehyde through a six-membered-ring transition state (white and upper cycle). Alternatively, a radical generated at $\alpha$-C will produce the diphenylethanone **1b** (dark and lower cycle).

**Role of the $CuO_x$ Clusters in the Reaction.** Furthermore, we studied the role of the $CuO_x$ clusters on the reaction. Previous theoretical calculations and experimental studies have suggested that the photocatalytic performance of ceria is associated with the surface oxygen vacancies and $Ce^{3+}$ ions.[25b,31] Copper oxides could increase surface oxygen vacancies and $Ce^{3+}$ ions of ceria in the case of $CuO_x/CeO_2$.[32] $Ce^{3+}$ ions are generated by reducing $Ce^{4+}$ ions when the oxygen vacancy is created.[33] The concentration of surface oxygen vacancies can be semiquantified by Raman spectroscopy.[14,34] We adopted a method[35] by using the Raman peak centered at 462 $cm^{-1}$ to estimate the oxygen vacancy concentration of ceria. The results are presented in Figure 5b. The oxygen vacancy concentration of pristine ceria is $3.58 \times 10^{21}$ $cm^{-3}$. A higher value of $5.88 \times 10^{21}$ $cm^{-3}$ is obtained when ceria is highly dispersed in nanosized domains on anatase nanotubes. More oxygen vacancies ($6.04 \times 10^{21}$ $cm^{-3}$) are generated after mixing copper oxide with ceria.

Next we measured the UV–vis DRS to study the optical properties of photocatalysts (Figure 6). A-NTs have no significant absorption of visible light, owing to the large energy gap. However, the addition of ceria extends the absorption of the resulting catalysts to visible light, which was also observed by other studies.[31a,b] This visible absorption enhancement



DOI: 10.1021/acscatal.7b00629
ACS Catal. 2017, 7, 3850–3859

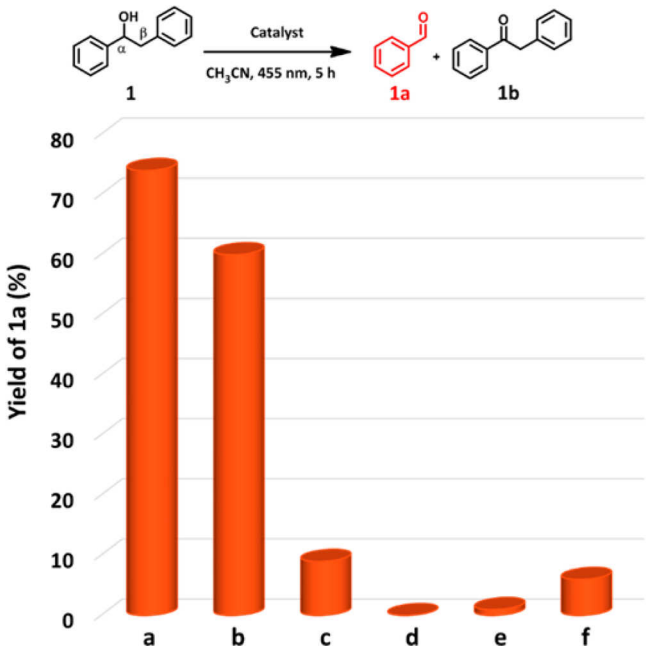


**Figure 4.** Influence of the reaction atmosphere and scavenger. Reaction conditions: substrate **1** (0.05 mmol), $CuO_x$/ceria/A-NTs (10 mg), $CH_3CN$ (1.0 mL), reaction pressure (1 atm), additive (0.05 mmol), 9.6 W LED (centered at 455 nm), room temperature, 5 h. The yield of **1a** was determined by GC with *n*-dodecane as the internal standard. (a, d–f) Reaction under $O_2$. (b) Reaction in air. (c) Reaction under Ar. (d) Reaction with *p*-benzoquinone as scavenger for superoxide radical. (e) Reaction with $(NH_4)_2C_2O_4$ as the scavenger for photogenerated holes. (f) Reaction with $K_2S_2O_8$ as the scavenger for photogenerated electrons.

**Scheme 4. Possible Mechanism**

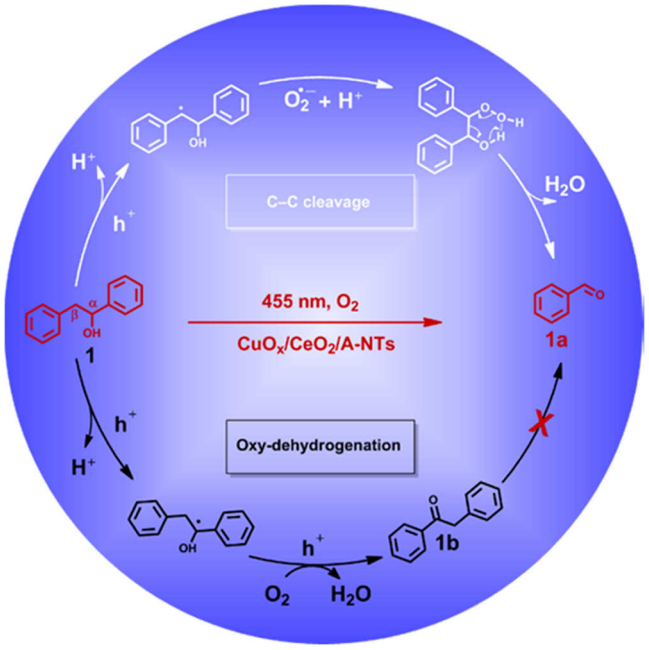


could be attributed to the existence of oxygen vacancies and $Ce^{3+}$ ions. The positive correlation between absorption at 455 nm and the concentration of oxygen vacancies and $Ce^{3+}$ ions for ceria-based photocatalysts further confirms this point (Figure 6a). The calculated band gaps of the as-prepared samples using a transformed Kubelka–Munk plot are shown in Figure 6b.[36] The optical band energies of ceria/A-NTs and $CuO_x$/ceria/A-NTs are calculated to be 2.72 and 2.62 eV, respectively, which are lower than that of pristine ceria (2.86

**Scheme 3. Control Experiment and Kinetic Isotope Effects (KIEs)**

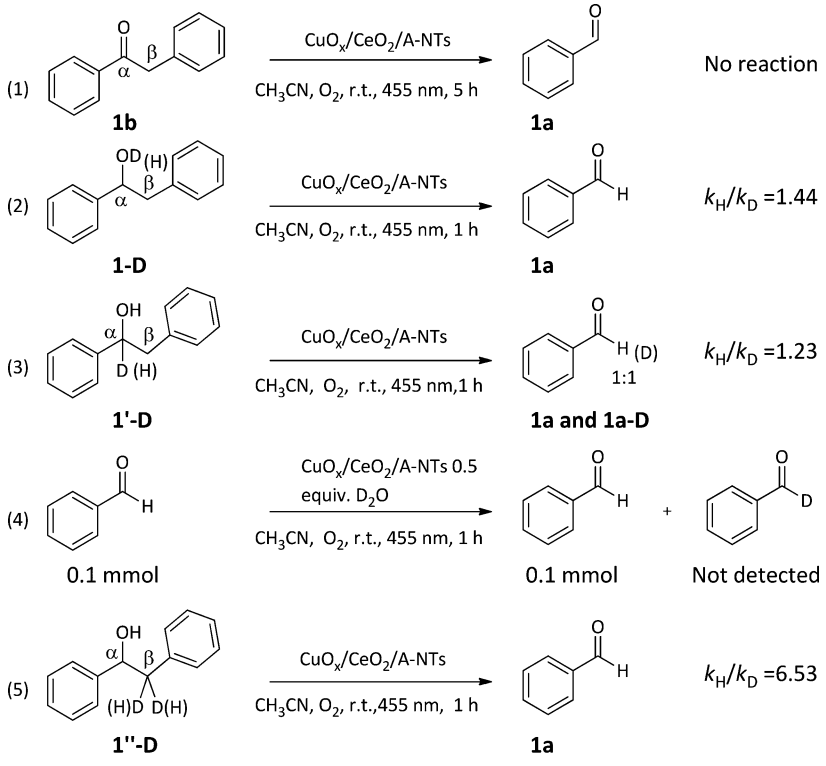




DOI: 10.1021/acscatal.7b00629
*ACS Catal.* 2017, 7, 3850–3859

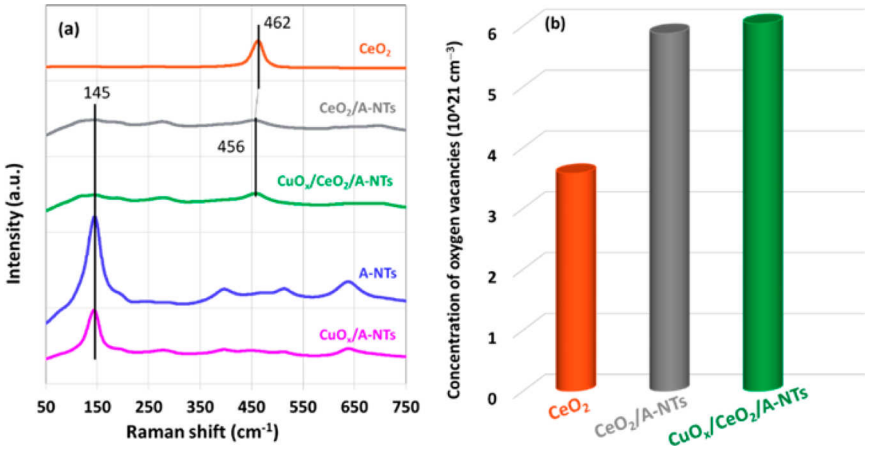


**Figure 5.** Raman spectra (a) and the oxygen vacancy concentrations (b) of the photocatalysts.

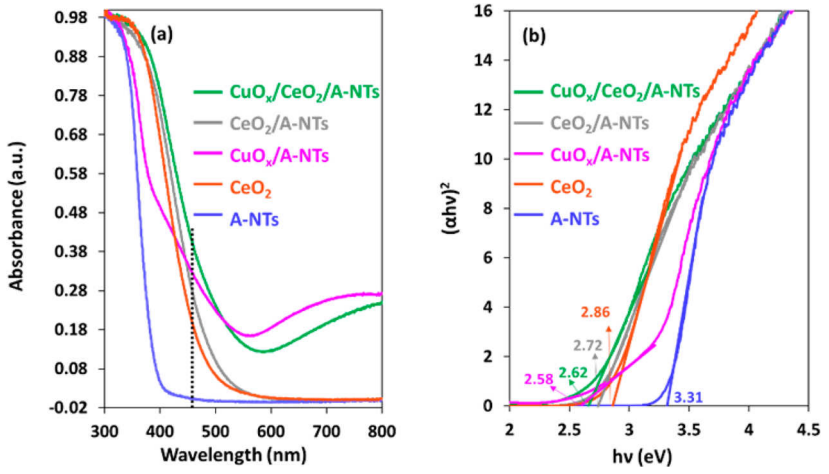


**Figure 6.** (a) UV−vis diffuse reflectance spectra and (b) optical adsorption edges of the ceria, A-NT, ceria/A-NT, $CuO_x$/A-NT, and $CuO_x$/ceria/A-NT photocatalysts, respectively.

eV). The presence of $Ce^{3+}$ leads to a narrowing of the band gap of ceria. The $CuO_x$ clusters present on the ceria domains increase the concentration of surface defects ($Ce^{3+}$ ions and oxygen vacancies), which we term its Yang character. For $CuO_x$/A-NTs, the band gap is 2.58 eV, lower than that of A-NTs. This result suggests that copper oxide electronically modifies anatase nanotubes, which agrees with XRD, STEM, and Raman spectroscopy results.

$CuO_x$/A-NTs showed no photocatalytic activity toward C−C bond cleavage. We then conducted a photocatalytic reaction under 365 nm UV light (Figure 7), under which electron−hole pairs of A-NTs can be excited. Consequently, a 16% yield of **1b** is obtained, together with a 22% yield of **1a**, indicating that both C−C bond cleavage and oxy-dehydrogenation reactions occur on anatase. Because ceria has no photocatalytic ability of oxy-dehydrogenation, it is very likely that the oxy-dehydrogenation reaction mainly occurs on A-NTs. The decoration of copper oxides on A-NTs can remarkably suppress the side reaction, decreasing the yield of **1b** to 4%, which we term the Yin character of $CuO_x$ clusters. We further compare the activities of the ceria/A-NTs and $CuO_x$/ceria/A-NTs under 365 nm UV light. The yield of **1a** increases from 27% to 36%, and the yield of **1b** decreases from 10% to 3%, which further confirms the Yin (inhibit the side oxy-dehydrogenation reaction) and Yang (enhance the C−C cleavage activity) dual

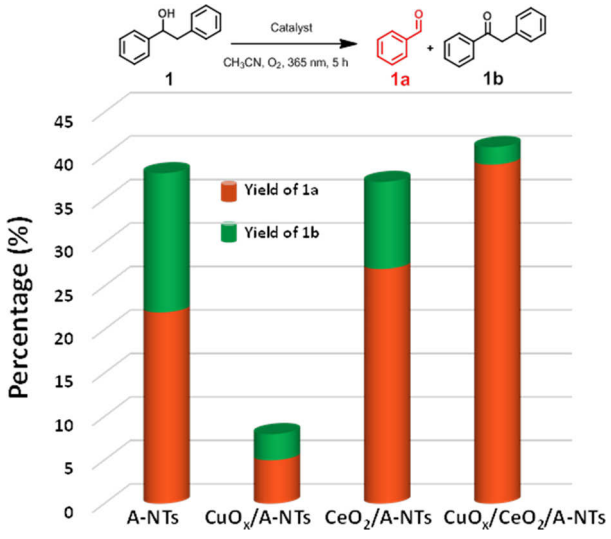


**Figure 7.** Photocatalytic reaction under UV light. Reaction conditions: substrate (0.05 mmol), catalyst (10 mg), $CH_3CN$ (1.0 mL), $O_2$ (1 atm), 6 W LED (centered at 365 nm), room temperature, 5 h. The yields were determined by GC with *n*-dodecane as the internal standard.



DOI: 10.1021/acscatal.7b00629
*ACS Catal.* 2017, 7, 3850−3859

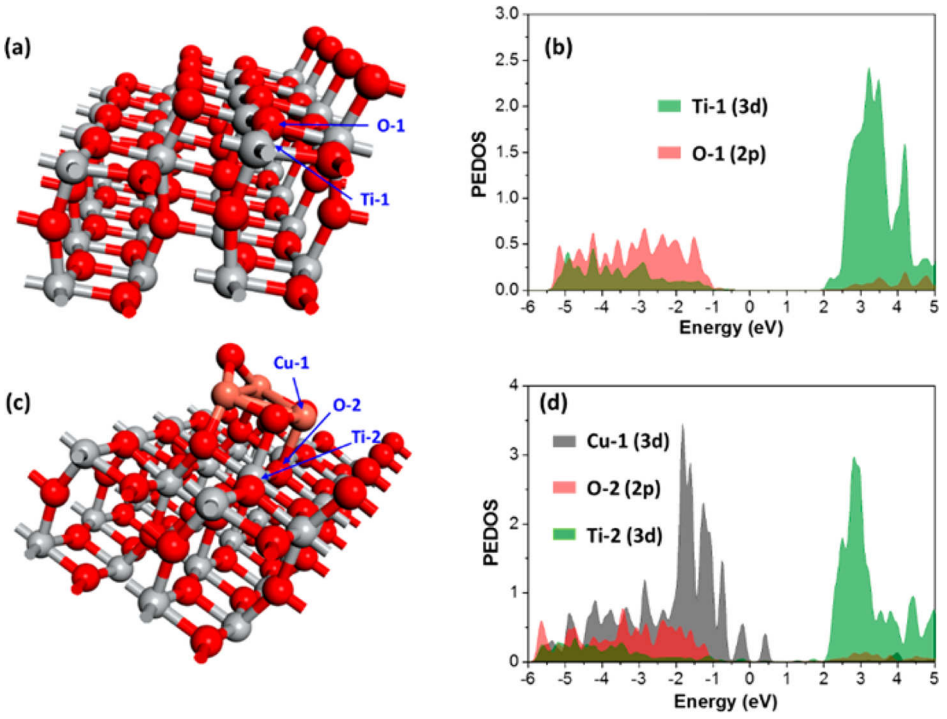


**Figure 8.** Atomic structure and calculated partial electronic density of states (PEDOS) for anatase (101) and $Cu_3O_3$/anatase (101), respectively.

characters of the $CuO_x$. Tada's group has observed that, with an increasing loading amount of $NiO_x$ or $CuO_x$ nanoclusters on $TiO_2$, the activity of photodegradation of organics decreased.[26a,37] In this work, we find that the photocatalytic oxydehydrogenation reaction on anatase fades away with an increase in the amount of $CuO_x$ to 2 wt % (Table S2 in the Supporting Information).

To further understand the Yin character of $CuO_x$ nanoclusters, we calculated the partial electronic density of states (PEDOS) of $CuO_x$/anatase using $Cu_3O_3$/anatase (101) as a model by DFT, in which Cu 3d, O 2p, and Ti 3d PEDOS are displayed (Figure 8). New states are present above the valence band edge of the anatase (101) surface (Figure 8d), which arise from the presence of $CuO_x$-derived occupied states that lie at higher energy than the VB edge of the anatase. The upward shift in the VB edge results in a narrowing of the band gap in comparison to unmodified $TiO_2$, which is consistent with the UV−vis results. Moreover, a rise in the VB edge will lead to a decrease in the activity of holes. As a result, the oxydehydrogenation reaction occurring on anatase is suppressed (Figure 7). This result is consistent with the case of $NiO_x$ or $CuO_x$ nanoclusters supported on $TiO_2$ reported by Nolan and Tada's group.[26a,37,38]

## CONCLUSIONS

In conclusion, we report a strategy of controlling $CuO_x$ cluster distribution on ceria/anatase nanotubes and the catalytic consequence in the model lignin C−C bond cleavage reaction. $CuO_x$/ceria/A-NT photocatalyst shows high activity in the C−C bond cleavage to benzaldehydes under visible light irradiation. Highly dispersed $CuO_x$ clusters on ceria domains enhance the $Ce^{3+}$ concentration in ceria and thus increase the catalytic activity (Yang character); the decoration of $CuO_x$ on the exposed anatase surface suppresses the unwanted oxydehydrogenation reaction by shifting the valence band edge of $TiO_2$ to higher energy (Yin character). Thus, a high photocatalytic performance is achieved under visible light. Hydrogen abstraction by photogenerated holes is involved in the reaction mechanism. We believe this work is instructive for the design of active photocatalysts for oxidation of C−C bonds and valorization of lignin and can also be used in broad organic reactions.

## ASSOCIATED CONTENT

### Supporting Information

The Supporting Information is available free of charge on the ACS Publications website at DOI: 10.1021/acscatal.7b00629.

Catalyst characterization, including TEM images and physical absorption, the effect of the copper amount on photocatalytic C−C bond cleavage, and the procedure for synthesis of model compounds (NMR characterization was also involved) (PDF)

## AUTHOR INFORMATION

### Corresponding Author

*F.W.: tel, +86-411-84379762; fax, +86-411-84379798; e-mail, wangfeng@dicp.ac.cn.

### ORCID

Tingting Hou: 0000-0002-6516-1548
Nengchao Luo: 0000-0002-6137-292X
Feng Wang: 0000-0002-9167-8743

### Notes

The authors declare no competing financial interest.

## ACKNOWLEDGMENTS

This work was supported by the National Natural Science Foundation of China (21422308, 21690082, 21690084) and the Strategic Priority Research Program of Chinese Academy of Sciences (XDB17020300). Computing resources from the National Supercomputing Center in Shenzhen (China) and



DOI: 10.1021/acscatal.7b00629
ACS Catal. 2017, 7, 3850−3859

National Supercomputing Center in Tianjin (China) are gratefully acknowledged.

## REFERENCES


(1) (a) Zhang, L.; Bi, X.; Guan, X.; Li, X.; Liu, Q.; Barry, B. D.; Liao, P. *Angew. Chem.* **2013**, *125*, 11513−11517. (b) Souillart, L.; Cramer, N. *Chem. Rev.* **2015**, *115*, 9410−9464. (c) Huang, X.; Li, X.; Zou, M.; Song, S.; Tang, C.; Yuan, Y.; Jiao, N. *J. Am. Chem. Soc.* **2014**, *136*, 14858−14865. (d) Wang, M.; Lu, J.; Zhang, X.; Li, L.; Li, H.; Luo, N.; Wang, F. *ACS Catal.* **2016**, *6*, 6086−6090.

(2) Bharathi, K.; Ravindra, P. *Electron. J. Environ., Agric. Food Chem.* **2006**, *5*, 1253−1264.

(3) Sedai, B.; Díaz-Urrutia, C.; Baker, R. T.; Wu, R.; Silks, L. A. P.; Hanson, S. K. *ACS Catal.* **2013**, *3*, 3111−3122.

(4) Luo, F. X.; Zhou, T. G.; Li, X.; Luo, Y. L.; Shi, Z. J. *Org. Chem. Front.* **2015**, *2*, 1066−1070.

(5) Wang, M.; Li, L. H.; Lu, J. M.; Li, H. J.; Zhang, X. C.; Liu, H. F.; Luo, N. C.; Wang, F. *Green Chem.* **2017**, *19*, 702−706.

(6) (a) Tomita, O.; Otsubo, T.; Higashi, M.; Ohtani, B.; Abe, R. *ACS Catal.* **2016**, *6*, 1134−1144. (b) Higashi, M.; Domen, K.; Abe, R. *J. Am. Chem. Soc.* **2013**, *135*, 10238−10241. (c) Abe, R.; Shinmei, K.; Koumura, N.; Hara, K.; Ohtani, B. *J. Am. Chem. Soc.* **2013**, *135*, 16872−16884. (d) Barreca, D.; Fornasiero, P.; Gasparotto, A.; Gombac, V.; Maccato, C.; Montini, T.; Tondello, E. *ChemSusChem* **2009**, *2*, 230−233.

(7) (a) Gombac, V.; Sordelli, L.; Montini, T.; Delgado, J. J.; Adamski, A.; Adami, G.; Cargnello, M.; Bernal, S.; Fornasiero, P. *J. Phys. Chem. A* **2010**, *114*, 3916−3925. (b) Okunaka, S.; Tokudome, H.; Hitomi, Y.; Abe, R. *J. Mater. Chem. A* **2015**, *3*, 1688−1695. (c) Yamauchi, M.; Abe, R.; Tsukuda, T.; Kato, K.; Takata, M. *J. Am. Chem. Soc.* **2011**, *133*, 1150−1152. (d) Abe, R.; Takami, H.; Murakami, N.; Ohtani, B. *J. Am. Chem. Soc.* **2008**, *130*, 7780−7781. (e) Yurdakal, S.; Palmisano, G.; Loddo, V.; Augugliaro, V.; Palmisano, L. *J. Am. Chem. Soc.* **2008**, *130*, 1568−1569.

(8) (a) Nguyen, J. D.; Matsuura, B. S.; Stephenson, C. R. *J. Am. Chem. Soc.* **2014**, *136*, 1218−1221. (b) Karkas, M. D.; Bosque, I.; Matsuura, B. S.; Stephenson, C. R. *Org. Lett.* **2016**, *18*, 5166−5169. (c) Gazi, S.; Hung Ng, W. K.; Ganguly, R.; Putra Moeljadi, A. M.; Hirao, H.; Soo, H. S. *Chem. Sci.* **2015**, *6*, 7130−7142.

(9) (a) Reddy, G. V. B.; Sridhar, M.; Gold, M. H. *Eur. J. Biochem.* **2003**, *270*, 284−292. (b) Wang, M.; Lu, J.; Ma, J.; Zhang, Z.; Wang, F. *Angew. Chem., Int. Ed.* **2015**, *54*, 14061−14065. (c) Cho, S. H.; Kim, J. Y.; Kwak, J.; Chang, S. *Chem. Soc. Rev.* **2011**, *40*, 5068−83.

(10) (a) Zhang, C.; Lu, J.; Zhang, X.; MacArthur, K.; Heggen, M.; Li, H.; Wang, F. *Green Chem.* **2016**, *18*, 6545−6555. (b) Kim, S.; Chmely, S. C.; Nimlos, M. R.; Bomble, Y. J.; Foust, T. D.; Paton, R. S.; Beckham, G. T. *J. Phys. Chem. Lett.* **2011**, *2*, 2846−2852.

(11) (a) Lim, S. H.; Lee, W. S.; Kim, Y.-I.; Sohn, Y.; Cho, D. W.; Kim, C.; Kim, E.; Latham, J. A.; Dunaway-Mariano, D.; Mariano, P. S. *Tetrahedron* **2015**, *71*, 4236−4247. (b) Cho, D. W.; Parthasarathi, R.; Pimentel, A. S.; Maestas, G. D.; Park, H. J.; Yoon, U. C.; Dunaway-Mariano, D.; Gnanakaran, S.; Langan, P.; Mariano, P. S. *J. Org. Chem.* **2010**, *75*, 6549−62.

(12) In Chinese philosophy, Yin means the negative principle (characterized by dark) and Yang means the positive principle (characterized by light) of the two opposing cosmic forces. Yin and Yang describe how seemingly opposite or contrary forces may actually be complementary, interconnected, and interdependent in the natural world and how they may give rise to each other as they interrelate to one another. In this work, the decoration of $CuO_x$ clusters could suppress the oxy-dehydrogenation reaction, which we term Yin character, and promoted the C−C bond cleavage, which we term Yang character.

(13) (a) Tsai, C.; Teng, H. *Chem. Mater.* **2004**, *16*, 4352−4358. (b) Zhao, H.; Dong, Y.; Jiang, P.; Wang, G.; Zhang, J. *ACS Appl. Mater. Interfaces* **2015**, *7*, 6451−6461.

(14) Wang, Y.; Wang, F.; Song, Q.; Xin, Q.; Xu, S.; Xu, J. *J. Am. Chem. Soc.* **2013**, *135*, 1506−1515.

(15) Kresse, G.; Furthmuller, J. *Comput. Mater. Sci.* **1996**, *6*, 15−50.

(16) Perdew, J. P.; Burke, K.; Ernzerhof, M. *Phys. Rev. Lett.* **1996**, *77*, 3865.

(17) Kresse, G.; Joubert, D. *Phys. Rev. B: Condens. Matter Mater. Phys.* **1999**, *59*, 1758−1775.

(18) Monkhorst, H. J.; Pack, J. D. *Phys. Rev. B* **1976**, *13*, 5188−5192.

(19) Dudarev, S. L.; Botton, G. A.; Savrasov, S. Y.; Humphreys, C. J.; Sutton, A. P. *Phys. Rev. B: Condens. Matter Mater. Phys.* **1998**, *57*, 1505−1509.

(20) Burdett, J. K.; Hughbanks, T.; Miller, G. J.; Richardson, J. W.; Smith, J. V. *J. Am. Chem. Soc.* **1987**, *109*, 3639−3646.

(21) (a) Kresse, G.; Furthmuller, J. *Phys. Rev. B: Condens. Matter Mater. Phys.* **1996**, *54*, 11169−11186. (b) Kresse, G.; Furthmuller, J. *Comput. Mater. Sci.* **1996**, *6*, 15−50.

(22) Perdew, J. P.; Burke, K.; Ernzerhof, M. *Phys. Rev. Lett.* **1996**, *77*, 3865−3868.

(23) (a) Kresse, G.; Joubert, D. *Phys. Rev. B: Condens. Matter Mater. Phys.* **1999**, *59*, 1758−1775. (b) Blochl, P. E. *Phys. Rev. B: Condens. Matter Mater. Phys.* **1994**, *50*, 17953−17979.

(24) (a) Jiang, D.; Wang, W.; Zhang, L.; Zheng, Y.; Wang, Z. *ACS Catal.* **2015**, *5*, 4851−4858. (b) Khan, M. M.; Ansari, S. A.; Pradhan, D.; Han, D. H.; Lee, J.; Cho, M. H. *Ind. Eng. Chem. Res.* **2014**, *53*, 9754−9763.

(25) (a) Younis, A.; Chu, D.; Kaneti, Y. V.; Li, S. *Nanoscale* **2016**, *8*, 378−387. (b) Zhao, K.; Qi, J.; Yin, H.; Wang, Z.; Zhao, S.; Ma, X.; Wan, J.; Chang, L.; Gao, Y.; Yu, R.; Tang, Z. *J. Mater. Chem. A* **2015**, *3*, 20465−20470. (c) Andersson, D. A.; Simak, S. I.; Johansson, B.; Abrikosov, I. A.; Skorodumova, N. V. *Phys. Rev. B: Condens. Matter Mater. Phys.* **2007**, *75*, 035109. (d) Montini, T.; Melchionna, M.; Monai, M.; Fornasiero, P. *Chem. Rev.* **2016**, *116*, 5987−6041.

(26) (a) Jin, Q.; Fujishima, M.; Iwaszuk, A.; Nolan, M.; Tada, H. *J. Phys. Chem. C* **2013**, *117*, 23848−23857. (b) Assadi, M. H. N.; Hanaor, D. A. H. *Appl. Surf. Sci.* **2016**, *387*, 682−689.

(27) Tang, C.; Jiao, N. *Angew. Chem., Int. Ed.* **2014**, *53*, 6528−6532.

(28) When the reaction was conducted under 365 nm light illumination, the substrate **1a** was dehydrogenated to **1b** as the major product over A-NTs, as shown in Figure 8.

(29) Zhao, J.; Chen, H.; Tian, X.; Zang, H.; Fu, Y.; Shen, J. *J. Catal.* **2013**, *298*, 161−169.

(30) (a) Raza, F.; Park, J. H.; Lee, H.; Kim, H.; Jeon, S.; Kim, J. *ACS Catal.* **2016**, *6*, 2754−2759. (b) Lang, X.; Ji, H.; Chen, C.; Ma, W.; Zhao, J. *Angew. Chem., Int. Ed.* **2011**, *50*, 3934−3937. (c) Su, F.; Mathew, S. C.; Mohlmann, L.; Antonietti, M.; Wang, X.; Blechert, S. *Angew. Chem., Int. Ed.* **2011**, *50*, 657−660.

(31) (a) Luo, S.; Nguyen-Phan, T.-D.; Johnston-Peck, A. C.; Barrio, L.; Sallis, S.; Arena, D. A.; Kundu, S.; Xu, W.; Piper, L. F. J.; Stach, E. A.; Polyanskiy, D. E.; Fujita, E.; Rodriguez, J. A.; Senanayake, S. D. *J. Phys. Chem. C* **2015**, *119*, 2669−2679. (b) Wang, Y.; Zhao, J.; Wang, T.; Li, Y.; Li, X.; Yin, J.; Wang, C. *J. Catal.* **2016**, *337*, 293−302. (c) Kundu, S.; Ciston, J.; Senanayake, S. D.; Arena, D. A.; Fujita, E.; Stacchiola, D.; Barrio, L.; Navarro, R. M.; Fierro, J. L. G.; Rodriguez, J. A. *J. Phys. Chem. C* **2012**, *116*, 14062−14070. (d) Catlow, C. R.; Guo, Z. X.; Miskufova, M.; Shevlin, S. A.; Smith, A. G.; Sokol, A. A.; Walsh, A.; Wilson, D. J.; Woodley, S. M. *Philos. Trans. R. Soc., A* **2010**, *368*, 3379−456.

(32) Knauth, P.; Saltsburg, H.; Engel, J.; Tuller, H. L. *J. Mater. Chem. A* **2015**, *3*, 8369−8379.

(33) (a) Lee, Y.; He, G.; Akey, A. J.; Si, R.; Flytzani-Stephanopoulos, M.; Herman, I. P. *J. Am. Chem. Soc.* **2011**, *133*, 12952−12955. (b) Esch, F.; Fabris, S.; Zhou, L.; Montini, T.; Africh, C.; Fornasiero, P.; Comelli, G.; Rosei, R. *Science* **2005**, *309*, 752−755.

(34) (a) Wu, Z.; Li, M.; Howe, J.; Meyer, H. M., III; Overbury, S. H. *Langmuir* **2010**, *26*, 16595−16606. (b) Li, M.; Tumuluri, U.; Wu, Z.; Dai, S. *ChemSusChem* **2015**, *8*, 3651−3660. (c) Wu, Z.; Li, M.; Overbury, S. H. *ChemCatChem* **2012**, *4*, 1653−1661. (d) Zhang, L.; Wu, Z.; Nelson, N. C.; Sadow, A. D.; Slowing, I. I.; Overbury, S. H. *ACS Catal.* **2015**, *5*, 6426−6435. (e) Zhang, Z.; Wang, Y.; Wang, M.; Lu, J.; Li, L.; Zhang, Z.; Li, M.; Jiang, J.; Wang, F. *Chin. J. Catal.* **2015**, *36*, 1623−1630. (f) Zhang, Z.; Wang, Y.; Wang, M.; Lu, J.; Zhang, C.; Li, L.; Jiang, J.; Wang, F. *Catal. Sci. Technol.* **2016**, *6*, 1693−1700.




DOI: 10.1021/acscatal.7b00629
*ACS Catal.* 2017, 7, 3850−3859

(35) (a) Deori, K.; Gupta, D.; Saha, B.; Deka, S. *ACS Catal.* **2014**, *4*, 3169−3179. (b) Trogadas, P.; Parrondo, J.; Ramani, V. *ACS Appl. Mater. Interfaces* **2012**, *4*, 5098−5102.
(36) Saavedra, J.; Doan, H. A.; Pursell, C. J.; Grabow, L. C.; Chandler, B. D. *Science* **2014**, *345*, 1599−1602.
(37) Iwaszuk, A.; Nolan, M.; Jin, Q.; Fujishima, M.; Tada, H. *J. Phys. Chem. C* **2013**, *117*, 2709−2718.
(38) (a) Fronzi, M.; Iwaszuk, A.; Lucid, A.; Nolan, M. *J. Phys.: Condens. Matter* **2016**, *28*, 074006. (b) Nolan, M.; Iwaszuk, A.; Lucid, A. K.; Carey, J. J.; Fronzi, M. *Adv. Mater.* **2016**, *28*, 5425−5446.



DOI: 10.1021/acscatal.7b00629
*ACS Catal.* 2017, 7, 3850−3859